KIF4A and PP2A–B56 form a spatially restricted feedback loop opposing Aurora B at the anaphase central spindle

Ricardo Nunes Bastos, Michael J. Cundell, and Francis A. Barr

Department of Biochemistry, University of Oxford, Oxford OX1 3QU, England, UK

The mitotic kinase Aurora B is concentrated at the anaphase central spindle by the kinesin MKlp2 during mitotic exit and cytokinesis. This pool of Aurora B phosphorylates substrates including the kinesin KIF4A to regulate central spindle length. In this paper, we identify a counteracting system in which PP2A–B56γ and -ε, but not PP2A–B56α, -β, and -δ, are maintained at the central spindle by KIF4A. Biochemical assays show that PP2A–B56γ can dephosphorylate the T799 Aurora B site on KIF4A and thereby counteract the Aurora B–and microtubule-stimulated ATPase activity of KIF4A. In agreement with these observations, combined silencing of PP2A–B56γ and -ε resulted in increased phosphorylation of KIF4A T799 and decreased central spindle growth in anaphase B. Furthermore, reduced turnover of regulatory phosphorylation on another Aurora B substrate MKlp1 was observed, suggesting that PP2A–B56γ and -ε play a general role opposing Aurora B at the central spindle. KIF4A and PP2A–B56γ and -ε therefore create a spatially restricted negative feedback loop counteracting Aurora B in anaphase.

Introduction

Anaphase central spindle formation is controlled by a group of conserved microtubule-associated proteins and kinesin motors (Barr and Gruneberg, 2007; Glotzer, 2009; Brust-Mascher and Scholey, 2011; Duellberg et al., 2013). Key among these are the antiparallel microtubule-stabilizing factor PRC1 and a microtubule dynamic instability suppressing kinesin KIF4A, which work together to create microtubule overlaps of defined length (Bringmann et al., 2004; Bieling et al., 2010; Subramanian et al., 2010; Hu et al., 2011). These microtubule overlaps are further stabilized by the centralspindlin complex formed by the MKlp1/KIF23 kinesin-like motor protein and the Cyk-4/MgcRacGAP Rho family GTPase regulator (Mishima et al., 2002; Douglas et al., 2010). Both PRC1 and centralspindlin are inhibited until anaphase onset by Cdk1–cyclin B phosphorylation (Jiang et al., 1998; Mollinari et al., 2002; Mishima et al., 2004; Zhu et al., 2006; Neef et al., 2007). At the onset of anaphase, PP2A–B55 removes the inhibitory Cdk1 phosphorylation on PRC1, triggering central spindle formation only after chromosome separation has commenced (Cundell et al., 2013). Together, these factors can explain the Cdk1-regulated decrease in microtubule catastrophe observed toward the cell equator in anaphase (Brust-Mascher et al., 2004; Cheerambathur et al., 2007). However, Cdk regulation of these components does not provide an obvious means to fine-tune microtubule dynamic instability in a spatially restricted manner and thereby promote anaphase B spindle elongation (Cheerambathur et al., 2007). In addition to negative regulation by Cdk1, all these components are subject to activating phosphorylations by either Aurora B or Plk1 (Polo-like kinase 1). PRC1 and centralspindlin phosphorylation by Plk1 are necessary for division plane specification (Neef et al., 2007; Petronczki et al., 2007; Wolfe et al., 2009). Aurora B phosphorylation of KIF4A at T799 activates its microtubule-stimulated ATPase activity and enhances KIF4A binding to PRC1, and the antiparallel microtubule overlap bundling activity of MKlp1 is promoted by Aurora B phosphorylation at S911 (Douglas et al., 2010; Nunes Bastos et al., 2013). KIF4A and MKlp1 are phosphorylated by a pool of Aurora B transported to the central spindle by the mitotic kinesin MKlp2 (Gruneberg et al., 2004; Neef et al., 2006; Ruchaud et al., 2007; Fuller et al., 2008; Brust-Mascher and Scholey, 2011; Nunes Bastos et al., 2013). Although, in both cases, previous studies

Correspondence to Francis A. Barr: francis.barr@bioch.ox.ac.uk

The Rockefeller University Press $30.00
J. Cell Biol. Vol. 207 No. 6 683–693
www.jcb.org/cgi/doi/10.1083/jcb.201409129

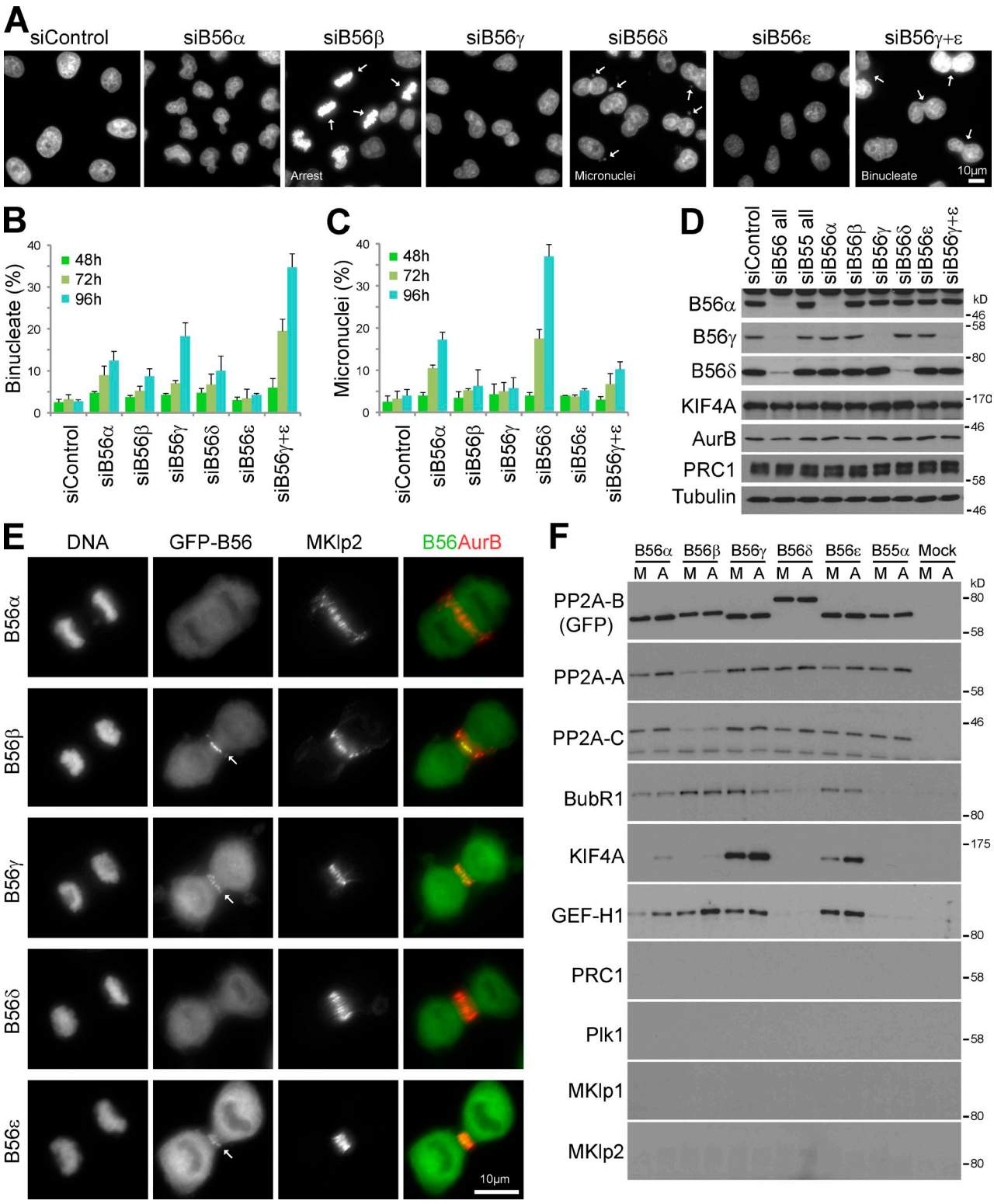

Figure 1. **Identification of isoform-specific components of PP2A–B56 complexes.** (A) HeLa cells treated with control and B56 regulatory subunit siRNA for 48–96 h were stained for DNA. Arrows indicate mitotically arrested, micronucleated, and binucleated cells. (B and C) Bar graphs show the frequency of binucleate (B) and micronucleated cells (C; means ± SEM, $n = 2$ measuring >200 cells per experiment). (D) Blots to confirm depletion of endogenous B56 regulatory subunits. KIF4A was used as a loading control and marker for mitosis. (E) Thymidine-synchronized HeLa cells were transfected with GFP-tagged PP2A–B56 regulatory subunits for 18 h, and then, the thymidine was washed out to allow the cells to enter mitosis. After 10 h, these cells were stained for DNA, mouse anti–Aurora B, and sheep anti-MKlp2. PP2A–B56 was visualized by GFP fluorescence. Arrows mark PP2A–B56 associated with the central spindle. (F) PP2A–B56 and –B55α complexes were isolated using GFP antibodies from metaphase (M) and anaphase (A) HeLa cells. Untransfected cells were used as a negative control (Mock). The immune precipitates (IP) were blotted, and the blots are representative of four independent experiments. siControl, control siRNA.

have shown that these phosphorylations have a short half-life (Neef et al., 2006; Nunes Bastos et al., 2013), until now, the KIF4A and MKlp1 phosphatases required for this dynamic behavior have not been identified. Analysis of Aurora B and Plk1 opposing phosphatases in chromosome alignment and spindle checkpoint signaling indicates that PP2A–B56 enzymes fulfill this requirement (Foley et al., 2011; Suijkerbuijk et al., 2012; Kruse et al., 2013). Because of these findings, the potential role of PP2A–B56 family enzymes as Aurora B–opposing phosphatases regulating central spindle dynamics during anaphase was investigated.

Results and discussion

Identification of isoform-specific components of PP2A-B56 complexes

Human cells express five different PP2A–B56 holoenzymes differentiated by the regulatory subunit (Shi, 2009; Wurzenberger and Gerlich, 2011). To determine whether these holoenzymes are associated with anaphase-specific functions, HeLa cells were depleted of the different B56 regulatory subunits. Binucleate cells were observed after silencing of B56γ, and this increased further when B56ε was silenced in combination (Fig. 1, A and B). B56α- and -δ–depleted cells showed increased nuclear abnormalities including micronucleation, and B56β-depleted cells arrested in mitosis with aligned chromosomes (Fig. 1, A and C). Blotting with the available isoform-specific antibodies confirmed depletion of B56α, -γ, and -δ subunits alone and in combination (Fig. 1 D). Other antibodies tested for B56β and -ε failed to show isoform-specific reactivity.

The localizations of the different B56 regulatory subunits were then investigated. Comparison with the anaphase central spindle proteins Aurora B and MKlp2 showed that B56β, -γ, and -ε gave a similar pattern of localization although an additional cytoplasmic distribution was visible (Fig. 1 E and Videos 1–3). B56α and -δ regulatory subunits showed only a diffuse localization (Fig. 1 E and Video 4). Thus, a subset of PP2A–B56 isoforms localize to the anaphase central spindle, consistent with supplemental data presented in a study of PP2A–B56 function in kinetochore fiber formation (Foley et al., 2011). These results suggest that B56γ and -ε function in anaphase or cytokinesis, whereas B56α, -β, and -δ may be more critical for chromosome alignment and segregation.

PP2A–B56 complexes were isolated from metaphase and anaphase cells (Fig. S1, A and B). Blotting showed that the different holoenzymes were isolated with approximately equivalent efficiency judged by the enrichment of both PP2A-A scaffold and PP2A-C catalytic subunits (Fig. 1 F). Mass spectrometry of the isolated protein complexes confirmed the equivalence of the different holoenzyme complexes (Fig. S1 C) and revealed the presence of the known PP2A–B56 interaction partners BubR1 and CDCA2/Repo-Man (Fig. S1 D; Suijkerbuijk et al., 2012; Kruse et al., 2013; Qian et al., 2013). In addition, two central spindle proteins, KIF4A and GEF-H1, were identified (Kurasawa et al., 2004; Birkenfeld et al., 2007). KIF4A was found in both B56γ and -ε complexes, with a slight enrichment in anaphase compared with metaphase samples (Figs. 1 F and S1 D). This behavior correlates with central spindle targeting of these holoenzymes (Fig. 1 E). The absence of the other major central spindle proteins PRC1, Plk1, MKlp1, and MKlp2 in B56γ and -ε complexes indicates that this is a specific property of KIF4A (Figs. 1 F and S1 D). GEF-H1 was detected in all PP2A–B56 complexes other than those formed by B56δ (Figs. 1 F and S1 D). This does not match the central spindle localization pattern of B56 isoforms and indicates that GEF-H1 is unlikely to be a central spindle–targeting factor for PP2A–B56. The simplest explanation for these observations was that KIF4A may act as a central spindle–targeting factor and substrate for PP2A–B56γ and -ε in anaphase. Both these possibilities were tested.

Central spindle localization of PP2A-B56γ and -ε is KIF4A dependent

Cells depleted of KIF4A failed to show the anaphase central spindle staining of PP2A–B56γ and -ε observed in control cells (Fig. 2 A). This was a highly reproducible and penetrant effect seen in nearly 90% of KIF4A-depleted cells (Fig. 2, B and C). Central spindle targeting of PP2A–B56β was not altered in KIF4A-depleted cells (Fig. 2, A and B). This was consistent with the mass spectrometry and Western blot data showing KIF4A was present only in PP2A–B56γ and -ε complexes (Figs. 1 B and S1 D). KIF4A therefore promotes central spindle targeting of PP2A–B56γ and -ε in anaphase, and PP2A–B56β targets to the central spindle by a KIF4A-independent mechanism.

PP2A-B56γ is a KIF4A pT799 Aurora B site phosphatase

In anaphase, Aurora B phosphorylates KIF4A on T799 and increases its microtubule-stimulated ATPase activity as part of the mechanism controlling central spindle length (Nunes Bastos et al., 2013). To test whether PP2A–B56γ acts directly on this site and modulates kinesin motor activity, Aurora B phosphorylated KIF4A (KIF4A pT799) was incubated with purified PP2A–B56γ, –B56β, or –B55α (Fig. 3 A). These PP2A complexes purified from interphase cells contain equal amounts of PP2A catalytic and scaffold subunits but lack detectable PP1 (Fig. 3 B). PP2A–B56γ rapidly dephosphorylated KIF4A pT799 but showed little activity toward PRC1 pT481 and pT602 (Fig. 3, A and C). The related enzyme PP2A–B56β, although present at the central spindle, was not active toward KIF4A pT799 (Fig. 3, A and C). In addition, KIF4A pT799 was not dephosphorylated by PP2A–B55α, although this enzyme was capable of dephosphorylating the pT481 Cdk1 site on PRC1 (Fig. 3, A and C), as expected (Cundell et al., 2013). Correlating with their activities toward pT799, PP2A–B56γ, and not B55α, reversed the effect of Aurora B phosphorylation on microtubule-stimulated KIF4A ATPase activity (Fig. 3 D).

The relationship between the two KIF4A-interacting forms of PP2A–B56 and the level of pT799 phosphorylation at the central spindle was then investigated. Because of their roles in error correction during mitotic spindle formation and spindle checkpoint silencing (Foley et al., 2011; Suijkerbuijk et al., 2012; Kruse et al., 2013), cells depleted of all B56 regulatory subunits arrested in a prometaphase-like state with

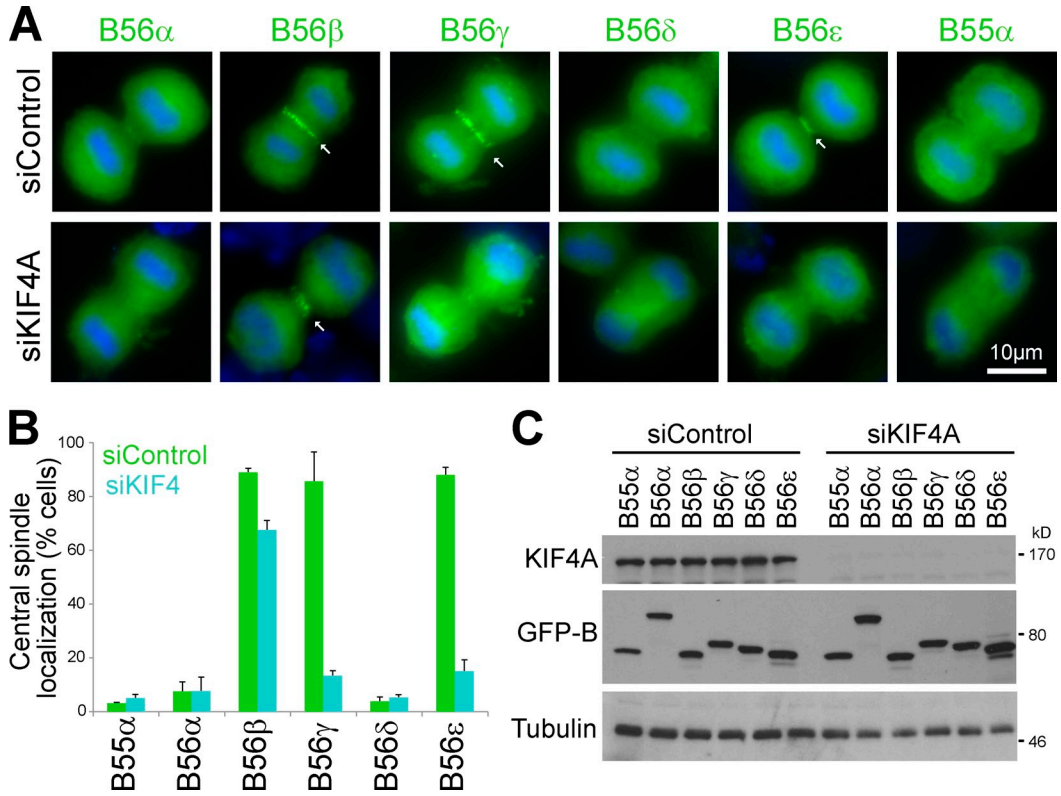

Figure 2. **KIF4A is required to target PP2A–B56γ and -ε to the central spindle.** (A) Thymidine-synchronized HeLa cells were transfected with GFP-tagged PP2A–B56 regulatory subunits and KIF4A siRNA for 24 h, and then, the thymidine was washed out. After 10 h, the cells were stained for DNA. PP2A–B56 was visualized by GFP fluorescence. Arrows mark PP2A–B56 associated with the central spindle. (B) Central spindle localization of GFP-tagged PP2A–B56 subunits in control and KIF4A silenced cells is plotted on a bar graph (means ± SEM, n = 3 measuring >100 cells per experiment). (C) Blots to confirm KIF4A depletion and expression of GFP-tagged PP2A–B56 subunits. Tubulin was used as a loading control. siControl, control siRNA.

scattered chromatin and failed to enter anaphase. Likewise, cells depleted of B56β arrested in a prometaphase-like state (Fig. 1, A and B), and the time from nuclear envelope breakdown to anaphase onset when observed was 250 ± 25 min (n = 50), compared with 63 ± 12 min (n = 30) for the control. Because of these defects in anaphase entry, it was not possible to analyze the effects of combined depletion of all central spindle isoforms of B56. The KIF4A-dependent central spindle–targeted B56 regulatory subunits γ and ε were therefore silenced individually or in combination. Depletion of B56γ or -ε singly resulted in a slight elevation of pT799 staining, and this was increased when both B56γ and -ε were depleted (Fig. 3, E and F). This effect was not observed in cells depleted of B56δ (Fig. 3, E and F), which is not present on the central spindle but does appear to be required for chromosome segregation because lagging chromatin and micronucleation were observed (Figs. 3 E and 1, A–C). The requirement for B56γ and -ε for turnover of the MKlp1 pS911 Aurora B phosphorylation was then tested. Although pS911 staining was not elevated in B56γ- and -ε–depleted cells, suggesting it is maximally phosphorylated, it failed to turn over after 5 min of Aurora B inhibition (Fig. S2, A and B). Similarly to KIF4A pT799, pS911 turnover involved a combination of both B56γ and -ε. These experiments show that PP2A–B56γ can directly dephosphorylate the pT799 Aurora B site on KIF4A, modulating its microtubule-stimulated ATPase activity, and that PP2A–B56γ and -ε act together to regulate turnover of Aurora B phosphorylations at the central spindle in vivo. Furthermore, they suggest that PP2A–B56γ specificity for KIF4A isn't solely determined by colocalization of both proteins at the central spindle, indicating that PP2A–B56 isoforms recognize specific determinants in their substrates.

KIF4A dynamics at the central spindle are regulated by PP2A-B56γ and -ε

Because KIF4A ATPase activity and PRC1 interaction are promoted by Aurora B phosphorylation (Nunes Bastos et al., 2013), loss of the pT799 phosphatase should cause increased levels of KIF4A at the central spindle. Moreover, inhibition of Aurora B should no longer result in the release of KIF4A from the central spindle. Live cell imaging of cells stably expressing EGFP-KIF4A confirmed both of these predictions. In cells depleted of PP2A–B56γ and -ε, the level of EGFP-KIF4A at the central spindle was increased by a little over twofold (Fig. 4, A and B). After Aurora B inhibition, EGFP-KIF4A was released from the central spindle in control cells but not in PP2A–B56γ- and -ε–depleted cells (Fig. 4, A and C). Importantly, the chromatin-associated pool of KIF4A, which is not regulated by Aurora B phosphorylation, was not altered by any of these manipulations. FRAP was then performed to analyze the binding of EGFP-KIF4A to the central spindle and chromatin (Fig. 4 D). Because the bleached volumes contain

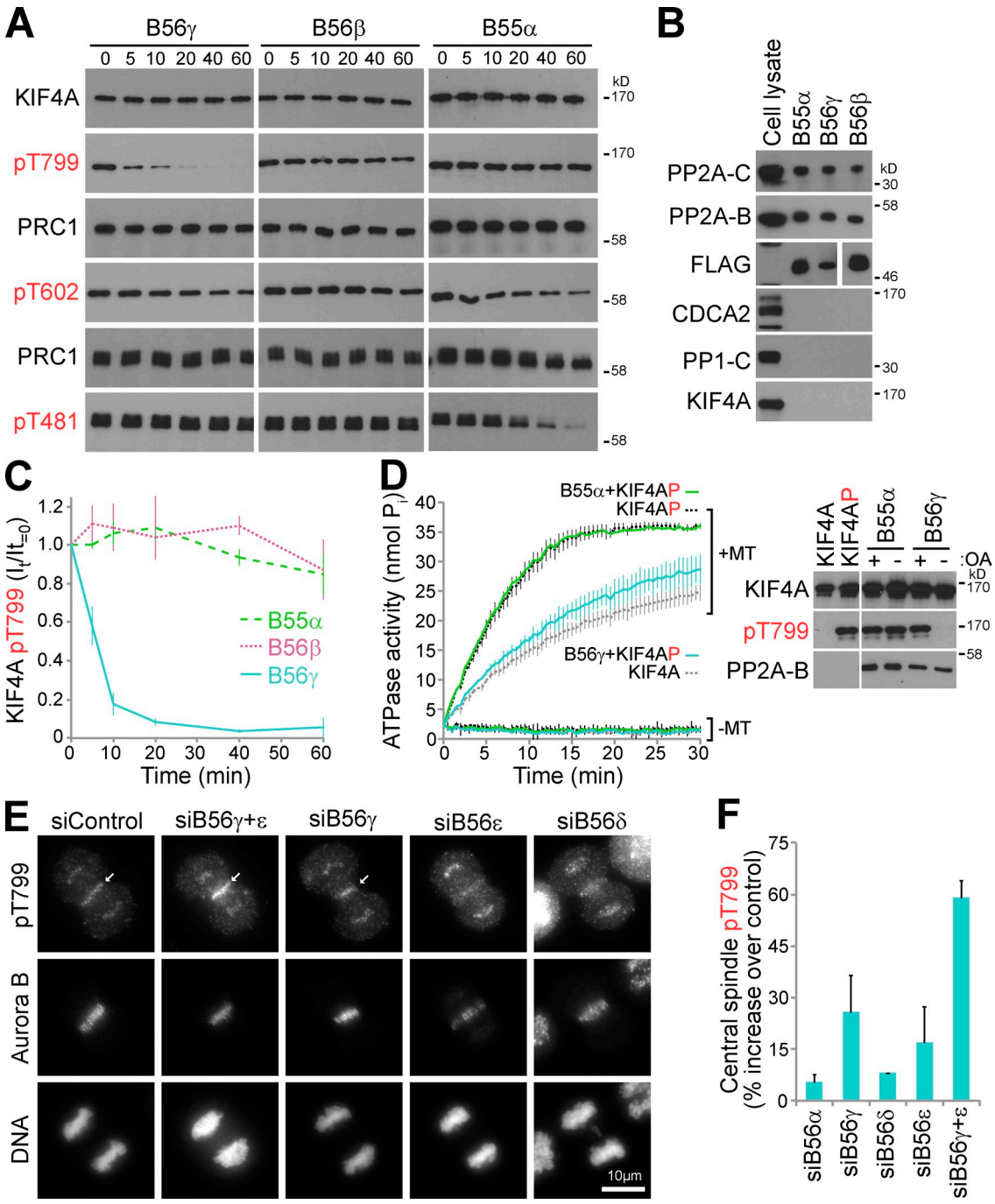

Figure 3. **PP2A–B56γ is a KIF4A pT799 phosphatase.** (A) Purified PP2A–B55α, –B56γ, and -β holoenzymes were tested for activity against recombinant KIF4A pT799, PRC1 pT481, or pT602 at 4°C for 0–60 min. Samples were blotted for the total and phosphorylated forms of the proteins. (B) Blots of purified PP2A holoenzymes and total cell lysate. (C) PP2A–B55α, –B56γ, and -β activity toward KIF4A pT799 is plotted on line graphs (means ± SEM, n = 2). Signal intensity for each time point (I_t) is plotted relative to t = 0 as $I_t/I_{t=0}$. (D) Kinesin ATPase assays were performed in the presence or absence of microtubules (±MT) using 100 nM KIF4A, Aurora B–phosphorylated KIF4A (KIF4AP), and KIF4AP treated with 1 nM PP2A–B56γ or B55α. Blotting confirmed the phosphorylation status of KIF4AP after 30-min treatment with PP2A–B55α or –B56γ in the presence (+) or absence (−) of okadaic acid (OA). White lines indicate that intervening lanes have been spliced out. (E) HeLa cells were treated with PP2A–B56 regulatory subunit siRNA for 24 h and then arrested with thymidine for 18 h. After 10 h, these cells were stained for DNA, mouse anti–Aurora B, and rabbit anti-KIF4A pT799. Arrows mark the central spindle pT799 signal. (F) Increased KIF4A pT799 staining relative to the control value is plotted in the bar graph (means ± SEM, n = 3 measuring >80 cells per condition).

both cytoplasmic and central spindle or chromatin-associated EGFP-KIF4A, a two-component model was used to fit the data. In both control and PP2A–B56γ- and -ε–depleted cells EGFP-KIF4A showed rapid recovery at the central spindle with a half-life of 10–11 s (Fig. 4 E). However, the mobile fraction was reduced from 62% to 47% in PP2A–B56γ- and -ε–depleted cells (Fig. 4 E), consistent with the idea that KIF4A binding sites are near saturation in the PP2A–B56γ- and -ε–depleted cells as a result of decreased dephosphorylation and dissociation of KIF4A from the central spindle. Recovery at the chromatin

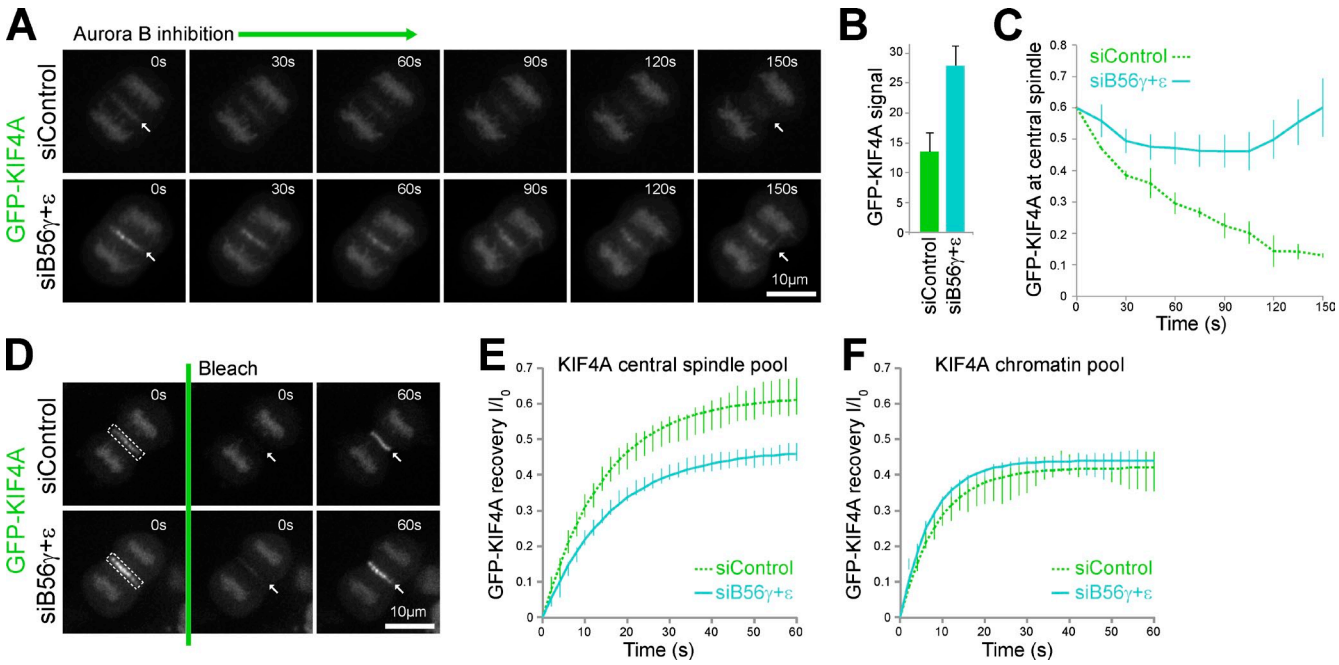

Figure 4. **KIF4A turnover at the central spindle is regulated by PP2A–B56γ and -ε.** (A) An EGFP-KIF4A HeLa cell line was treated with control or combined PP2A–B56γ and -ε siRNA for 36 h, arrested with 2 mM thymidine for 18 h, and then released for 8 h into fresh medium before imaging every 30 s as the cells passed through mitosis and cytokinesis. When cells in the field of view were in anaphase A, 1 µM ZM447439 was added to inhibit Aurora B and imaging, then continued during anaphase B. Arrows mark the central spindle region. (B) Central spindle staining intensity of EGFP-KIF4A in control and PP2A–B56γ and -ε silenced cells is plotted in the bar graph (mean ± SEM, *n* = 3). (C) Relative EGFP-KIF4A signal at the central spindle after Aurora B inhibition is plotted as a function of time on the line graph (means ± SEM, *n* = 3). (D) Turnover of EGFP-KIF4A was measured in control and PP2A–B56γ and -ε silenced cells using FRAP. In the example shown, the central spindle to be bleached is indicated by the dotted boxed areas, and arrows mark the recovering signal. (E and F) Turnover of the EGFP-KIF4A components at the central spindle (E) and chromosomes (F) are plotted in the line graphs (means ± SEM, *n* = 3).

was the same under both conditions with a half-life of 5–6 s and identical mobile fraction (Fig. 4 F), indicating that association and dissociation were unaltered. PP2A–B56γ and -ε may therefore control the release of KIF4A from the central spindle by localized dephosphorylation. Further support for this view was obtained from a mathematical model defining all these biochemical reactions (Fig. S3, A and B). This model describes the accumulation of phosphorylated KIF4A (Cp) from a soluble cytoplasmic pool (K) on spindle microtubules as cells enter anaphase (Fig. S3 C, solid lines). Reduction in the soluble pool of PP2A–B56 had little effect on spindle associated KIF4A and slightly increased soluble phosphorylated KIF4A (Fig. S3 C, dotted lines). KIF4A levels on spindle microtubules increased after the removal of the spindle-associated pool of PP2A–B56 corresponding to B56γ and -ε (Fig. S3 D), similar to experimental data (Fig. 4, A and B). Aurora B inhibition caused rapid loss of KIF4A (Cp) from spindle microtubules in control conditions (Fig. S3 E) but only a slow decline after reduction of the spindle associated PP2A–B56 activity (Fig. S3 F, enlarged region), fitting well with data obtained in cells (Fig. 4 C).

PP2A-B56γ and -ε regulation of anaphase central spindle length

Accumulation of phosphorylated KIF4A at the central spindle would be expected to suppress microtubule dynamics and prevent full extension of this structure (Nunes Bastos et al., 2013). In both control and PP2A–B56γ- and -ε–depleted cells, sister chromatid separation occurred without any obvious changes in anaphase A (Fig. 5 A and Videos 5 and 6). At this point, 4 min into anaphase, sister chromatids were separated by ∼4.0 ± 1.0 µm in both cases (Fig. 5 B). In anaphase B, from 4 to 11 min, the central spindle extended by a further 6 µm in control cells and by 3 µm, half this extent, in PP2A–B56γ- and -ε–depleted cells (Fig. 5 B and Videos 5 and 6). Similar findings were made using fixed populations of anaphase-enriched cells, in which combined depletion of B56γ and -ε reduced mean central spindle length from 8.3 ± 0.4 µm to 5.9 ± 0.4 µm (Fig. 5 C). This was not caused by loss of the central spindle because both PRC1 and Plk1 were still present in the expected positions and at the same levels (Fig. 5 C). Depletion of B56γ and -ε alone, or other B56 regulatory subunits, did not result in reduction of central spindle length (Fig. 5 C).

General principles of PP2A-B56 and Aurora B–regulated systems

The concept that coordinated pairs of kinases and phosphatases control key regulatory phosphosites is an emerging theme in cell cycle control (Foley et al., 2011; Suijkerbuijk et al., 2012; Kruse et al., 2013; Xu et al., 2013; Espert et al., 2014). As we show here, it is also important for understanding the dynamic nature of central spindle formation and remodeling in anaphase. Rapid central spindle growth in anaphase A is promoted by PRC1 and other factors and then followed by a slower expansion during anaphase B limited by KIF4A and Aurora B (Brust-Mascher

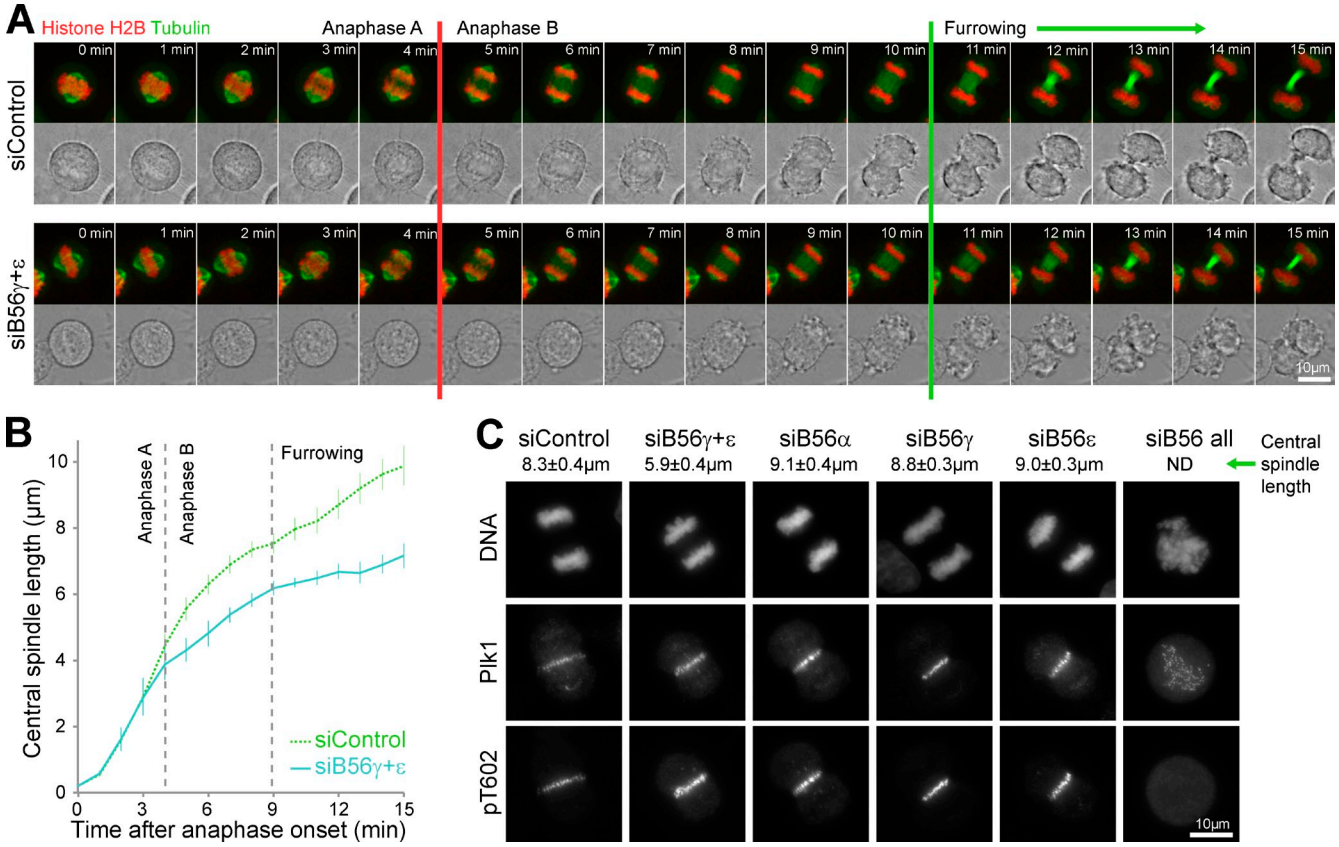

Figure 5. **PP2A–B56γ and -ε contribute to central spindle length control.** (A) HeLa EGFP-tubulin mCherry-histone H2B cells were treated with control or combined PP2A–B56γ and -ε siRNA for 36 h, arrested with 2 mM thymidine for 18 h, and then released for 8 h into fresh medium before imaging every minute as the cells passed through mitosis and cytokinesis. Red and green lines mark the anaphase A–B transition and onset of furrowing, respectively. (B) Central spindle length is plotted as a function of time (means ± SEM, *n* = 8). (C) HeLa cells were treated with control, combined PP2A–B56γ and -ε, PP2A–B56α, -γ, or -ε siRNA for 36 h, arrested with 2 mM thymidine for 18 h, and then released into fresh medium. After 10 h, these cells were stained for DNA, mouse anti-Plk1, and rabbit anti-PRC1 pT602. Central spindle length in anaphase cells is shown (means ± SEM, *n* = 6).

et al., 2004; Nunes Bastos et al., 2013). If there were no phosphatase opposing Aurora B, KIF4A phosphorylation would fail to turn over and microtubule dynamics would be completely suppressed. This problem is avoided because KIF4A-dependent maintenance of PP2A–B56γ and -ε Aurora B–counteracting phosphatases creates a negative feedback loop that allows slow central spindle elongation during anaphase B. It also potentially provides a mechanism to explain the spatial and temporal fine-tuning of microtubule dynamic instability at the cell equator in anaphase proposed previously (Cheerambathur et al., 2007).

This and previous work indicates that PP2A–B55 and PP2A–B56 have an inverse activity relationship toward Cdk and Aurora B sites (Cundell et al., 2013), therefore allowing independent regulation of these different dephosphorylation events. Other lines of evidence suggest that localized pools of PP2A–B56 act to oppose Aurora B more widely. In spindle checkpoint signaling, a BubR1-associated pool of PP2A–B56 opposes Aurora B and Mps1 at kinetochores (Foley et al., 2011; Suijkerbuijk et al., 2012; Kruse et al., 2013; Xu et al., 2013; Espert et al., 2014). In prometaphase, PP2A–B56 interacts with and dephosphorylates the Repo-Man PP1 complex at an Aurora B site, promoting its interaction with chromatin (Qian et al., 2013). Because PP1–Repo-Man dephosphorylates the Aurora B–chromosome passenger complex binding site on histone H3, this negatively regulates Aurora B binding to chromatin (Qian et al., 2011). In anaphase, the KIF4A-targeted pool of B56γ and -ε is ideally placed to counteract Aurora B phosphorylations on other central spindle proteins such as MKlp1. However, this complicates existing pictures of Aurora B function in anaphase, which typically envisage a gradient of Aurora B phosphorylation concentrated at the midpoint of the central spindle and minimal at either end (Fuller et al., 2008; Wang et al., 2011, 2013; Ferreira et al., 2013; Afonso et al., 2014). Although Aurora B and its counteracting phosphatases become spatially separated to permit dephosphorylation at chromatin (Wang et al., 2013; Afonso et al., 2014), as shown here, the presence of a phosphatase in the system with the same spatial distribution as the kinase is in fact necessary to explain the dynamic turnover of phosphorylation sites at the central spindle. Distribution of Aurora B alone is thus not the determining factor for phosphorylation of a given site. Instead, the functional outcome depends critically on the distribution of the counteracting phosphatase.

Materials and methods

Reagents and antibodies

General laboratory chemicals and reagents were obtained from Sigma-Aldrich and Thermo Fisher Scientific. Sheep antibodies were raised to MKlp1 (aa 1–444), KIF4A (full-length protein expressed in insect cells),

and MKlp2 (aa 63–193; Neef et al., 2003, 2007; Bastos and Barr, 2010; Nunes Bastos et al., 2013). Rabbit antibodies were raised to full-length recombinant PRC1, PRC1 pT602 peptide CILNS(pT)NIQS, KIF4A (aa 738–1,323), KIF4A pT799 peptide CLRRR(pT)FSLT, and MKlp1 pS911 peptide CRKRR(pS)STVA (Neef et al., 2003, 2006, 2007; Gruneberg et al., 2006; Nunes Bastos et al., 2013). Specific antibodies were purified using the antigens conjugated to Affi-Gel 15, eluted with 0.2 M glycine-HCl, pH 2.8, and then dialyzed against PBS before storage at −80°C. Commercially available antibodies were used to α-tubulin (mouse DM1A; Sigma-Aldrich), Plk1 (mouse SC-17783; Santa Cruz Biotechnology, Inc.), PRC1 pT481 (rabbit SC-11768 [Santa Cruz Biotechnology, Inc.] and rabbit monoclonal EP1514Y [Epitomics, Inc.]), the RGS-His tag epitope (mouse; QIAGEN), AIM1 (mouse 611083; BD), and cyclin B1 (mouse GNS3; EMD Millipore). Affinity-purified primary and secondary antibodies were used at 1 µg/ml final concentration. Donkey anti–mouse, –rabbit, or –sheep/goat secondary antibodies conjugated to HRP were obtained from Jackson ImmunoResearch Laboratories, Inc. Donkey anti–mouse, –rabbit, or –sheep/goat secondary antibodies conjugated to Alexa Fluor 488, 555, and 647 were obtained from Invitrogen. DNA was stained with DAPI (Sigma-Aldrich).

Kinase inhibitors were obtained from Tocris Bioscience (ZM447439; 10 mM 1,000× stock) and Axon Medchem (BI2536; 1 mM 1,000× stock). A benchtop microfuge (5417R; Eppendorf) was used for all centrifugations unless otherwise indicated.

Molecular biology

Human PP2A–B56α, -β, -γ, -δ, and -ε and PP2A–B55α were amplified from human testis cDNA (Marathon cDNA; Takara Bio Inc.) using Pfu polymerase (Agilent Technologies). Mammalian expression constructs for N-terminally FLAG or EGFP-tagged full-length KIF4A or PP2A–B56 subunits under the control of a tetracycline/doxycycline-inducible cytomegalovirus immediate-early enhancer/promoter joined with a dual-tetracycline operator sequence were made using the pcDNA5/FRT/TO vector (Invitrogen). The Baronase module was designed from existing crystal structures (Bayliss et al., 2003; Sessa et al., 2005) and created using standard molecular biology procedures to fuse human inner centromere protein aa 834–897 plus an additional glycine residue to the N terminus of Aurora B aa 44–344 (Nunes Bastos et al., 2013). For bacterial expression, this was expressed from pQE32 (QIAGEN) under the control of an isopropyl β-D-1-thiogalactopyranoside–inducible hybrid T5-phage/lac promoter. The pAcSG2 vector and BaculoGold system (Invitrogen) were used to create recombinant baculovirus carrying hexahistidine-tagged full-length PRC1 and KIF4A under the control of the *Autographa californica* nuclear polyhedrosis virus polyhedrin promoter. Primers were obtained from Invitrogen. The siRNA duplexes used to target PP2A and KIF4A listed in Table S1 were obtained from Thermo Fisher Scientific and have been described previously (Cundell et al., 2013; Nunes Bastos et al., 2013).

Human and insect cell culture

HeLa cells were cultured in DMEM containing 10% (vol/vol) bovine calf serum (Invitrogen) at 37°C and 5% CO_2. For synchronization, cells were treated for 18 h with 2 mM thymidine and washed three times in PBS and twice with growth medium. For plasmid transfection and siRNA transfection, Mirus LT1 (Mirus Bio LLC) and Oligofectamine (Invitrogen), respectively, were used. Stable HeLa cell lines with single copies of the desired transgene were created using the T-Rex doxycycline-inducible Flp-In system (Invitrogen). Sf9 insect cells were grown in insect cell growth medium (TC100 containing 10% [vol/vol] bovine calf serum and GlutaMAX [Invitrogen]) at 27°C and atmospheric CO_2.

Protein expression and preparation of phosphatase substrates

Recombinant baculoviruses encoding hexahistidine-tagged KIF4A, PRC1, and Plk1 were used to infect 4 × 10^7 insect cells in 20× 15-cm dishes with a multiplicity of infection of 10. To infect cells, the medium was removed, and the virus was added in 3 ml of insect growth medium per dish. Dishes were gently rocked for 1 h; every 10 min, the dishes were rotated by 90°. After 1 h, 17 ml insect cell growth medium was added, and the cells were left for 60 h before harvesting by centrifugation at 200 *g*. To obtain M-phase Cdk-phosphorylated PRC1, the cells were treated for 3 h with 100 nM okadaic acid before harvesting. Cell pellets were washed once in ice-cold PBS, and then lysed in 10 ml IMAC20 (20 mM Tris-HCl, pH 8.0, 300 mM NaCl, 20 mM imidazole, and 0.2% [vol/vol] Triton X-100) and protease inhibitor cocktail (Sigma-Aldrich) for 20 min on ice. Clarified cell lysate prepared by centrifugation at 100,000 *g* in a rotor (TLA100.3; Beckman Coulter) was loaded onto a 1-ml HisTrap FF column (GE Healthcare) at 0.5 ml/min. The column was then washed with 30 ml IMAC20 and eluted with a 20-ml linear gradient from 20 to 200 mM imidazole in IMAC20 collecting 1-ml fractions. Peak fractions judged by SDS-PAGE and absorbance at 280 nm were concentrated using Ultracel-10K centrifugal filters (EMD Millipore) according to the manufacturer's instructions to a final volume of ∼1 ml. Samples were then buffer exchanged using 5-ml desalt spin columns (Zeba; Perbio) into TND (20 mM Tris-HCl, pH 8, 300 mM NaCl, and 1 mM DTT). Protein samples were snap frozen in 15-µl aliquots and stored at −80°C for further use. To generate the PRC1-pT602 substrate lacking pT481 phosphorylation, 20 µg PRC1 purified from insect cells that had not been treated with okadaic acid, or nocodazole was phosphorylated in vitro by incubating with 1.2 µg Plk1 in a final volume of 50 µl of 20 mM Tris-HCl, pH 8.0, 150 mM NaCl, 1 mM DTT, and 3 mM Mg-ATP for 1 h at 37°C. The Baronase Aurora B mini-kinase fusion was expressed in *Escherichia coli* strain JM109 and purified in the same way, except that cell lysis was performed using a cell breaker system (EmulsiFlex C5; Avestin Europe GmbH). Aurora B–phosphorylated proteins were prepared by incubating 8 µg purified KIF4A with 1 µg Baronase and 1 mM Mg-ATP for 60 min at 37°C and then kept on ice until required.

Isolation of PPP complexes from metaphase and anaphase cells

Three 15-cm dishes of thymidine-synchronized HeLa S3 cells per condition were transfected for 18 h with GFP-tagged PP2A–B56 regulatory subunits then released for 6 h at 37°C, 100 ng/ml nocodazole was added, and they were incubated for a further 12–14 h. Mitotic cells were collected by shake-off, and nocodazole was removed by washing three times with PBS and twice with growth medium warmed to 37°C. Cells were left for 25 min at 37°C to form bipolar metaphase spindles (metaphase sample), and then 30 min after, the 200 µM AZ3146 was added, which causes rapid spindle checkpoint inactivation and progression into anaphase (anaphase sample). Cells were pelleted and washed three times with ice-cold PBS. Cell pellets were suspended in 1 ml mitotic lysis buffer (20 mM Tris-HCl, pH 7.4, 150 mM NaCl, 1% [vol/vol] IGEPAL, 0.1% [wt/vol] sodium deoxycholate, 40 mM β-glycerophosphate, 10 mM NaF, 0.3 mM Na-vanadate, 100 nM okadaic acid, and protease and phosphatase inhibitor cocktails [Sigma-Aldrich]), left for 15 min on ice, and then clarified by centrifugation at 20,000 g_{av} for 20 min at 4°C. Protein complexes were isolated from 3 mg of cell lysate using 3 µg sheep antibodies to GFP bound to 20 µl protein G Sepharose by incubation for 2 h at 4°C. Isolated complexes were washed once with lysis buffer and then three times with 20 mM Tris-HCl, pH 7.4, 150 mM NaCl, and 0.1% (vol/vol) IGEPAL. Samples were then analyzed by SDS-PAGE and blotting.

Isolation of PP2A–B55 and PP2A–B56 for phosphatase assays

HEK293T cells were seeded onto 15-cm dishes (7.325 × 10^6 cells per dish) and grown for 24 h. Seven dishes per condition were transiently transfected with 8 µg pcDNA5/FRT/TO FLAG (empty vector control), FLAG-PPP2R2A, or FLAG-PPP2R5C. After harvesting, cells were washed 3× in 50 ml ice-cold PBS, centrifuged at 400 *g* for 3 min at 4°C, and the pellets lysed in 2 ml ice-cold T-lysis buffer (20 mM Tris-HCl, pH 7.35, 150 mM NaCl, 1% [vol/vol] Triton X-100, and protease inhibitor cocktail [Sigma-Aldrich]) on ice for 15 min. Extracts were clarified at 20,817 *g* for 15 min at 4°C, supernatants were isolated, and then, 200 µl FLAG M2-agarose beads (Sigma-Aldrich) prewashed in T-lysis buffer was added per condition. After 3 h at 4°C, beads were washed 2× in T-lysis buffer, 4× in TBS (20 mM Tris-HCl, pH 7.35, and 150 mM NaCl) containing 0.1% (vol/vol) Triton X-100, 1× in TBS, and 1× in elution buffer (20 mM Tris-HCl, pH 7.35, 150 mM NaCl, and 1 mM $MnCl_2$). Bound proteins were eluted from beads in 110 µl elution buffer containing 200 µg/ml FLAG peptide (F3290; Sigma-Aldrich) at 22°C for 30 min. Glycerol ($[25\%]_{final}$) and DTT ($[1\ mM]_{final}$) were added to the eluate before aliquoting and snap freezing.

Mass spectrometry of PP2A–B56 complexes

Protein samples for mass spectrometry were separated on 4–12% gradient NuPAGE gels and then stained using a colloidal Coomassie blue stain. Gels were cut into six slices, and the proteins were digested with trypsin. The resulting tryptic peptide mixtures were then analyzed by online liquid chromatography–tandem mass spectrometry with an ultra-performance liquid chromatography system (Proxeon; Thermo Fisher Scientific) and mass spectrometer (Orbitrap Elite; Thermo Fisher Scientific) fitted with a nano-electrospray source (Thermo Fisher Scientific). The MaxQuant 1.5.0.35 quantitative proteomics software package was used to compile and search the raw data against the human UniProt database (Cox et al., 2009; Tyanova et al., 2014).

Activity assays with purified PP2A holoenzymes

Reactions were set up on ice and performed in tubes treated with a blocking buffer (50 mM Tris-HCl, pH 7.35, 0.1 mM $MnCl_2$, 1 mM $MgCl_2$, 1 mM DTT, 0.1% [vol/vol] IGEPAL, 150 mM NaCl, and 2 mg/ml BSA) to limit nonspecific loss of protein components on tube walls. Standard assays used 1.33 µg phosphorylated KIF4A or 3.0 µg PRC1 in 280 µl of reaction buffer (50 mM Tris-HCl, pH 7.35, 0.1 mM $MnCl_2$, 1 mM $MgCl_2$, 1 mM DTT, 0.1% [vol/vol] IGEPAL, 300 mM NaCl, and 0.2 mg/ml BSA). To start the reaction, PP2A holoenzyme was added, and the samples were incubated either at 4°C or 37°C. Samples were removed at the indicated time points, added to SDS sample buffer, and boiled immediately for 5 min to stop reactions.

Kinesin motor ATPase assays

A commercial enzyme linked inorganic phosphate assay was used to measure kinesin ATPase activity (Cytoskeleton, Inc.). In brief, a microtubule premix was created at room temperature by mixing 1 ml of reaction buffer (15 mM Pipes-KOH, pH 7, and 5 mM $MgCl_2$), 10 µl of 2 mM paclitaxel, 80 µl of preassembled microtubules (1 mg/ml tubulin, 15 mM Pipes-KOH, pH 7, 5 mM $MgCl_2$, 1 mM GTP, and 20 µM paclitaxel), 240 µl of 1 mM 2-amino-6-mercapto-7-methylpurine riboside, and 12 µl of 0.1 U/µl purine nucleoside phosphorylase. Phosphorylated KIF4A was prepared by preincubating the motor protein with 10 nM Baronase in a final volume of 7.5 µl TND containing 1 mM Mg-ATP for 30 min at 30°C and then adding 1 µM ZM447439 to stop the reaction. Dephosphorylation was performed using 1 nM recombinant PP2A–B56-γ for 30 min on ice and stopped by adding 1 µM okadaic acid. Reactions were set up in 96-well plates by mixing the protein of interest in a total volume of 7.5 µl TND with 147.5 µl of the microtubule premix at room temperature. To start the assay, 10 µl of 10 mM ATP was added to each well. Final assay volume was 165 µl of 12 mM Pipes-KOH, pH 7, 4 mM $MgCl_2$, 0.61 mM ATP, and 14.5 mM NaCl. This was then rapidly transferred to a 37°C plate reader (Tristar LB 941; Berthold Technologies) set to read absorbance at 360 nm. Readings were acquired every 30 s for 1 h. An inorganic phosphate standard curve was created in the same assay buffer and used to convert absorbance to nanomoles of ATP hydrolyzed.

Fixed and live cell microscopy

For fixed cell imaging, cells were grown on No. 1.5 glass coverslips (Menzel-Gläser; Thermo Fisher Scientific), washed twice with 2 ml PBS, and then fixed with 2 ml of 3% (wt/vol) paraformaldehyde in PBS for 15 min. Fixative was removed, and the cells were quenched with 2 ml of 50 mM NH_4Cl in PBS for 10 min. For the localization of GFP-tagged PP2A–B56 and –B55α, the cells were fixed in −20°C methanol for 7 min. Coverslips were washed three times in 2 ml PBS before permeabilization in 0.2% (vol/vol) Triton X-100 for 5 min. In all cases, primary and secondary antibody staining was performed in PBS for 60 min at room temperature. Affinity-purified antibodies were used at 1 µg/ml, whereas commercial antibodies were used as directed by the manufacturers. DAPI was added to the secondary antibody staining solution at 0.3 µg/ml. Coverslips were mounted in Mowiol 4–88 mounting medium (EMD Millipore). Fixed samples on glass slides were imaged using a 60×, NA 1.35 oil immersion objective on an upright microscope (BX61; Olympus) with filter sets for DAPI, GFP/Alexa Fluor 488, Alexa Fluor 555, Alexa Fluor 568, and Alexa Fluor 647 (Chroma Technology Corp.), a camera (CoolSNAP HQ2; Roper Scientific), and MetaMorph 7.5 imaging software (Molecular Devices). Illumination was provided by a metal halide light source (Lumen 200 Watt; Prior Scientific Instruments, Ltd.). Image stacks of 17 planes with a spacing of 0.6 µm through the cell volume were taken. Image stacks were maximum intensity projected and then merged to create 24-bit RGB TIFF files in MetaMorph. Images in 24-bit RGB format were then cropped in Photoshop CS3 and placed into Illustrator CS3 (Adobe) to produce the figures.

For live cell imaging using spinning-disk confocal microscopy, cells were plated in 35-mm dishes with a 14-mm No. 1.5 thickness coverglass window in the bottom (MatTek Corporation). For imaging, the dishes were placed in a 37°C and 5% CO_2 environment chamber (Tokai Hit) on the microscope stage. Imaging was performed at 37°C in 5% CO_2 using an inverted microscope (IX81; Olympus) with a 60×, 1.42 NA oil immersion objective coupled to a spinning-disk confocal system (UltraVIEW Vox; PerkinElmer) fitted with an electron-multiplying charge-coupled device camera (C9100-13; Hamamatsu Photonics). Exposure times were 30 ms for GFP-KIF4A using 4% laser power. Image stacks of 24 planes spaced 0.6 µm apart were taken at 1–4 stage positions every minute for ≤6 h. A bright-field reference image was also taken to visualize cell shape. Maximum intensity projection of the fluorescent channels was performed in Volocity (PerkinElmer) to create 24-bit RGB TIFF files.

KIF4A FRAP data acquisition and analysis

Prebleach five image stacks of four planes with 0.4-µm spacing were acquired at 1-s intervals. Bleach was performed using an UltraVIEW PhotoKinesis Device (PerkinElmer) with the 488-nm laser set at 10% with following settings: 5 cycles, step size of 1, spot period of 10, stop period of 10, 1 spot cycle, small spot size, and no attenuation. Recovery images were acquired for 60 time points every 2 s. Quantification and analysis of the FRAP data were performed using ImageJ (National Institutes of Health). Because the bleached volume contained both soluble cytoplasmic and central spindle central EGFP-KIF4A, data were analyzed using a two-component model. The normalized fluorescence intensity (I/I_o) as a function of time (t) for both components equals $A \times (1 - e^{-\tau t})$, in which A is the mobile fraction and τ is the rate constant. Images in 8-bit grayscale or 24-bit RGB TIFF format were then placed into Illustrator (Adobe) to produce the figures.

A mathematical model for KIF4A regulation in anaphase

The biochemical reactions providing the basis for the mathematical modeling are described in Fig. S3 A. KIF4A is present in soluble cytoplasmic (K) and central spindle associated fractions (C), which can also be phosphorylated (Kp and Cp). Aurora B kinase is described by the term A, k_{ph} and k_{dp} are rate constants for phosphorylation and dephosphorylation of KIF4A, and k_{MT} and k_d are rate constants for microtubule binding and release of KIF4A at the spindle. In the model, the time-dependent rate of change of each component is described by a nonlinear ordinary differential equation (Fig. S3 B). Each term on the right-hand side of the ordinary differential equation corresponds to a biochemical reaction. Because the values of the parameters (rate constants and relative protein levels) are largely unknown, they have to be estimated within reasonable bounds based on known details of the system. First, it can be assumed that $k_{ph} >> k_{ph1}$ because Aurora B is predominantly spindle associated, and $k_{dp} > k_{dp1}$ because B56 is enriched at spindle but also present in cytoplasm. A global parameter A represents the total activity of Aurora B in the system. Phosphorylation does not alter apparent microtubule binding in pelleting assays, so $k_{MT} = k_{MT1}$; however, phosphorylation increases microtubule residence time ($\ln(2)/k_d$), so $k_d < k_{d1}$. These parameters are set to A = 1, $k_{MT1} = 0.2$, $k_{d1} = 5$, $k_{ph} = 10$, $k_{dp} = 1.0$, $k_{MT} = 0.2$, $k_d = 0.1$, $k_{ph1} = 0.001$, and $k_{dp1} = 0.2$ for the control conditions. To mimic 95% depletion of B56γ and -ε, k_{dp} is reduced to 0.05, and because it is assumed to contribute 50% of soluble PP2A–B56, k_{dp1} is reduced to 0.1. To simulate the requirement for Aurora B, A was reduced to 0.1, equal to 90% inhibition. Because all available KIF4A is cytoplasmic at anaphase onset, K = 1 provides the starting condition for the simulation. Time series simulation and analysis of the model were performed with the freely available software XPPAUT (http://www.math.pitt.edu/~bard/xpp/xpp.html).

Online supplemental material

Fig. S1 shows additional characterization and mass spectrometry data for PP2A–B56 complexes. Fig. S2 shows the analysis of MKlp1 pS911 turnover after Aurora B inhibition. Fig. S3 provides details of the model explaining control of KIF4A by Aurora B and PP2A–B56. Table S1 lists siRNA duplexes used to target PP2A and KIF4A. Videos 1–4 show the localization of the different GFP-tagged PP2A–B56β, -γ, -ε, and -δ subunits, respectively, in cells passing from metaphase into anaphase and cytokinesis. Videos 5 and 6 show central spindle differences in control and PP2A–B56γ+ε–depleted cells, respectively. Online supplemental material is available at http://www.jcb.org/cgi/content/full/jcb.201409129/DC1. Additional data are available in the JCB DataViewer at http://dx.doi.org/10.1083/jcb.201409129.dv.

We thank Professor Bela Novak and Dr. Ulrike Gruneberg (Dunn School of Pathology, Oxford, England, UK) for much discussion and sharing unpublished observations and Josip Ahel for carefully reading the manuscript. We greatly appreciate the advice and assistance of Dr. Shabaz Mohammed in performing mass spectrometry of PP2A complexes.

A Cancer Research UK programme grant award (C20079/A15940) to F.A. Barr funded this work.

The authors declare no competing financial interests.

Submitted: 26 September 2014
Accepted: 18 November 2014

References

Afonso, O., I. Matos, A.J. Pereira, P. Aguiar, M.A. Lampson, and H. Maiato. 2014. Feedback control of chromosome separation by a midzone Aurora B gradient. *Science*. 345:332–336. http://dx.doi.org/10.1126/science.1251121

Barr, F.A., and U. Gruneberg. 2007. Cytokinesis: placing and making the final cut. *Cell*. 131:847–860. http://dx.doi.org/10.1016/j.cell.2007.11.011

Bastos, R.N., and F.A. Barr. 2010. Plk1 negatively regulates Cep55 recruitment to the midbody to ensure orderly abscission. *J. Cell Biol.* 191:751–760. http://dx.doi.org/10.1083/jcb.201008108

Bayliss, R., T. Sardon, I. Vernos, and E. Conti. 2003. Structural basis of Aurora-A activation by TPX2 at the mitotic spindle. *Mol. Cell*. 12:851–862. http://dx.doi.org/10.1016/S1097-2765(03)00392-7

Bieling, P., I.A. Telley, and T. Surrey. 2010. A minimal midzone protein module controls formation and length of antiparallel microtubule overlaps. *Cell*. 142:420–432. http://dx.doi.org/10.1016/j.cell.2010.06.033

Birkenfeld, J., P. Nalbant, B.P. Bohl, O. Pertz, K.M. Hahn, and G.M. Bokoch. 2007. GEF-H1 modulates localized RhoA activation during cytokinesis under the control of mitotic kinases. *Dev. Cell*. 12:699–712. http://dx.doi.org/10.1016/j.devcel.2007.03.014

Bringmann, H., G. Skiniotis, A. Spilker, S. Kandels-Lewis, I. Vernos, and T. Surrey. 2004. A kinesin-like motor inhibits microtubule dynamic instability. *Science*. 303:1519–1522. http://dx.doi.org/10.1126/science.1094838

Brust-Mascher, I., and J.M. Scholey. 2011. Mitotic motors and chromosome segregation: the mechanism of anaphase B. *Biochem. Soc. Trans.* 39:1149–1153. http://dx.doi.org/10.1042/BST0391149

Brust-Mascher, I., G. Civelekoglu-Scholey, M. Kwon, A. Mogilner, and J.M. Scholey. 2004. Model for anaphase B: role of three mitotic motors in a switch from poleward flux to spindle elongation. *Proc. Natl. Acad. Sci. USA*. 101:15938–15943. http://dx.doi.org/10.1073/pnas.0407044101

Cheerambathur, D.K., G. Civelekoglu-Scholey, I. Brust-Mascher, P. Sommi, A. Mogilner, and J.M. Scholey. 2007. Quantitative analysis of an anaphase B switch: Predicted role for a microtubule catastrophe gradient. *J. Cell Biol.* 177:995–1004. http://dx.doi.org/10.1083/jcb.200611113

Cox, J., I. Matic, M. Hilger, N. Nagaraj, M. Selbach, J.V. Olsen, and M. Mann. 2009. A practical guide to the MaxQuant computational platform for SILAC-based quantitative proteomics. *Nat. Protoc.* 4:698–705. http://dx.doi.org/10.1038/nprot.2009.36

Cundell, M.J., R.N. Bastos, T. Zhang, J. Holder, U. Gruneberg, B. Novak, and F.A. Barr. 2013. The BEG (PP2A-B55/ENSA/Greatwall) pathway ensures cytokinesis follows chromosome separation. *Mol. Cell*. 52:393–405. http://dx.doi.org/10.1016/j.molcel.2013.09.005

Douglas, M.E., T. Davies, N. Joseph, and M. Mishima. 2010. Aurora B and 14-3-3 coordinately regulate clustering of centralspindlin during cytokinesis. *Curr. Biol.* 20:927–933. http://dx.doi.org/10.1016/j.cub.2010.03.055

Duellberg, C., F.J. Fourniol, S.P. Maurer, J. Roostalu, and T. Surrey. 2013. End-binding proteins and Ase1/PRC1 define local functionality of structurally distinct parts of the microtubule cytoskeleton. *Trends Cell Biol.* 23:54–63. http://dx.doi.org/10.1016/j.tcb.2012.10.003

Espert, A., P. Uluocak, R.N. Bastos, D. Mangat, P. Graab, and U. Gruneberg. 2014. PP2A-B56 opposes Mps1 phosphorylation of Knl1 and thereby promotes spindle assembly checkpoint silencing. *J. Cell Biol.* 206:833–842. http://dx.doi.org/10.1083/jcb.201406109

Ferreira, J.G., A.J. Pereira, A. Akhmanova, and H. Maiato. 2013. Aurora B spatially regulates EB3 phosphorylation to coordinate daughter cell adhesion with cytokinesis. *J. Cell Biol.* 201:709–724. http://dx.doi.org/10.1083/jcb.201301131

Foley, E.A., M. Maldonado, and T.M. Kapoor. 2011. Formation of stable attachments between kinetochores and microtubules depends on the B56-PP2A phosphatase. *Nat. Cell Biol.* 13:1265–1271. http://dx.doi.org/10.1038/ncb2327

Fuller, B.G., M.A. Lampson, E.A. Foley, S. Rosasco-Nitcher, K.V. Le, P. Tobelmann, D.L. Brautigan, P.T. Stukenberg, and T.M. Kapoor. 2008. Midzone activation of aurora B in anaphase produces an intracellular phosphorylation gradient. *Nature*. 453:1132–1136. http://dx.doi.org/10.1038/nature06923

Glotzer, M. 2009. The 3Ms of central spindle assembly: microtubules, motors and MAPs. *Nat. Rev. Mol. Cell Biol.* 10:9–20. http://dx.doi.org/10.1038/nrm2609

Gruneberg, U., R. Neef, R. Honda, E.A. Nigg, and F.A. Barr. 2004. Relocation of Aurora B from centromeres to the central spindle at the metaphase to anaphase transition requires MKlp2. *J. Cell Biol.* 166:167–172. http://dx.doi.org/10.1083/jcb.200403084

Gruneberg, U., R. Neef, X. Li, E.H. Chan, R.B. Chalamalasetty, E.A. Nigg, and F.A. Barr. 2006. KIF14 and citron kinase act together to promote efficient cytokinesis. *J. Cell Biol.* 172:363–372. http://dx.doi.org/10.1083/jcb.200511061

Hu, C.K., M. Coughlin, C.M. Field, and T.J. Mitchison. 2011. KIF4 regulates midzone length during cytokinesis. *Curr. Biol.* 21:815–824. http://dx.doi.org/10.1016/j.cub.2011.04.019

Jiang, W., G. Jimenez, N.J. Wells, T.J. Hope, G.M. Wahl, T. Hunter, and R. Fukunaga. 1998. PRC1: a human mitotic spindle-associated CDK substrate protein required for cytokinesis. *Mol. Cell*. 2:877–885. http://dx.doi.org/10.1016/S1097-2765(00)80302-0

Kruse, T., G. Zhang, M.S. Larsen, T. Lischetti, W. Streicher, T. Kragh Nielsen, S.P. Bjørn, and J. Nilsson. 2013. Direct binding between BubR1 and B56-PP2A phosphatase complexes regulate mitotic progression. *J. Cell Sci.* 126:1086–1092. http://dx.doi.org/10.1242/jcs.122481

Kurasawa, Y., W.C. Earnshaw, Y. Mochizuki, N. Dohmae, and K. Todokoro. 2004. Essential roles of KIF4 and its binding partner PRC1 in organized central spindle midzone formation. *EMBO J.* 23:3237–3248. http://dx.doi.org/10.1038/sj.emboj.7600347

Mishima, M., S. Kaitna, and M. Glotzer. 2002. Central spindle assembly and cytokinesis require a kinesin-like protein/RhoGAP complex with microtubule bundling activity. *Dev. Cell*. 2:41–54. http://dx.doi.org/10.1016/S1534-5807(01)00110-1

Mishima, M., V. Pavicic, U. Grüneberg, E.A. Nigg, and M. Glotzer. 2004. Cell cycle regulation of central spindle assembly. *Nature*. 430:908–913. http://dx.doi.org/10.1038/nature02767

Mollinari, C., J.P. Kleman, W. Jiang, G. Schoehn, T. Hunter, and R.L. Margolis. 2002. PRC1 is a microtubule binding and bundling protein essential to maintain the mitotic spindle midzone. *J. Cell Biol.* 157:1175–1186. http://dx.doi.org/10.1083/jcb.200111052

Neef, R., C. Preisinger, J. Sutcliffe, R. Kopajtich, E.A. Nigg, T.U. Mayer, and F.A. Barr. 2003. Phosphorylation of mitotic kinesin-like protein 2 by polo-like kinase 1 is required for cytokinesis. *J. Cell Biol.* 162:863–875. http://dx.doi.org/10.1083/jcb.200306009

Neef, R., U.R. Klein, R. Kopajtich, and F.A. Barr. 2006. Cooperation between mitotic kinesins controls the late stages of cytokinesis. *Curr. Biol.* 16:301–307. http://dx.doi.org/10.1016/j.cub.2005.12.030

Neef, R., U. Gruneberg, R. Kopajtich, X. Li, E.A. Nigg, H. Sillje, and F.A. Barr. 2007. Choice of Plk1 docking partners during mitosis and cytokinesis is controlled by the activation state of Cdk1. *Nat. Cell Biol.* 9:436–444. http://dx.doi.org/10.1038/ncb1557

Nunes Bastos, R., S.R. Gandhi, R.D. Baron, U. Gruneberg, E.A. Nigg, and F.A. Barr. 2013. Aurora B suppresses microtubule dynamics and limits central spindle size by locally activating KIF4A. *J. Cell Biol.* 202:605–621. http://dx.doi.org/10.1083/jcb.201301094

Petronczki, M., M. Glotzer, N. Kraut, and J.M. Peters. 2007. Polo-like kinase 1 triggers the initiation of cytokinesis in human cells by promoting recruitment of the RhoGEF Ect2 to the central spindle. *Dev. Cell*. 12:713–725. http://dx.doi.org/10.1016/j.devcel.2007.03.013

Qian, J., B. Lesage, M. Beullens, A. Van Eynde, and M. Bollen. 2011. PP1/Repo-man dephosphorylates mitotic histone H3 at T3 and regulates chromosomal aurora B targeting. *Curr. Biol.* 21:766–773. http://dx.doi.org/10.1016/j.cub.2011.03.047

Qian, J., M. Beullens, B. Lesage, and M. Bollen. 2013. Aurora B defines its own chromosomal targeting by opposing the recruitment of the phosphatase scaffold Repo-Man. *Curr. Biol.* 23:1136–1143. http://dx.doi.org/10.1016/j.cub.2013.05.017

Ruchaud, S., M. Carmena, and W.C. Earnshaw. 2007. Chromosomal passengers: conducting cell division. *Nat. Rev. Mol. Cell Biol.* 8:798–812. http://dx.doi.org/10.1038/nrm2257

Sessa, F., M. Mapelli, C. Ciferri, C. Tarricone, L.B. Areces, T.R. Schneider, P.T. Stukenberg, and A. Musacchio. 2005. Mechanism of Aurora B activation by INCENP and inhibition by hesperadin. *Mol. Cell*. 18:379–391. http://dx.doi.org/10.1016/j.molcel.2005.03.031

Shi, Y. 2009. Serine/threonine phosphatases: mechanism through structure. *Cell*. 139:468–484. http://dx.doi.org/10.1016/j.cell.2009.10.006

Subramanian, R., E.M. Wilson-Kubalek, C.P. Arthur, M.J. Bick, E.A. Campbell, S.A. Darst, R.A. Milligan, and T.M. Kapoor. 2010. Insights into antiparallel microtubule crosslinking by PRC1, a conserved nonmotor microtubule binding protein. *Cell*. 142:433–443. http://dx.doi.org/10.1016/j.cell.2010.07.012

Suijkerbuijk, S.J., M. Vleugel, A. Teixeira, and G.J. Kops. 2012. Integration of kinase and phosphatase activities by BUBR1 ensures formation of stable kinetochore-microtubule attachments. *Dev. Cell*. 23:745–755. http://dx.doi.org/10.1016/j.devcel.2012.09.005

Tyanova, S., M. Mann, and J. Cox. 2014. MaxQuant for in-depth analysis of large SILAC datasets. *Methods Mol. Biol.* 1188:351–364. http://dx.doi.org/10.1007/978-1-4939-1142-4_24

Wang, E., E.R. Ballister, and M.A. Lampson. 2011. Aurora B dynamics at centromeres create a diffusion-based phosphorylation gradient. *J. Cell Biol.* 194:539–549. http://dx.doi.org/10.1083/jcb.201103044

Wang, H., I. Brust-Mascher, G. Civelekoglu-Scholey, and J.M. Scholey. 2013. Patronin mediates a switch from kinesin-13–dependent poleward flux to anaphase B spindle elongation. *J. Cell Biol.* 203:35–46. http://dx.doi.org/10.1083/jcb.201306001

Wolfe, B.A., T. Takaki, M. Petronczki, and M. Glotzer. 2009. Polo-like kinase 1 directs assembly of the HsCyk-4 RhoGAP/Ect2 RhoGEF complex to initiate cleavage furrow formation. *PLoS Biol.* 7:e1000110. http://dx.doi.org/10.1371/journal.pbio.1000110

Wurzenberger, C., and D.W. Gerlich. 2011. Phosphatases: providing safe passage through mitotic exit. *Nat. Rev. Mol. Cell Biol.* 12:469–482. http://dx.doi.org/10.1038/nrm3149

Xu, P., E.A. Raetz, M. Kitagawa, D.M. Virshup, and S.H. Lee. 2013. BUBR1 recruits PP2A via the B56 family of targeting subunits to promote chromosome congression. *Biol. Open*. 2:479–486. http://dx.doi.org/10.1242/bio.20134051

Zhu, C., E. Lau, R. Schwarzenbacher, E. Bossy-Wetzel, and W. Jiang. 2006. Spatiotemporal control of spindle midzone formation by PRC1 in human cells. *Proc. Natl. Acad. Sci. USA*. 103:6196–6201. http://dx.doi.org/10.1073/pnas.0506926103